Isotropic and kinematic hardening of a high entropy alloy

O. Bouaziz, Jongun Moon, Hyoung Seop Kim, Yuri Estrin

Isotropic and Kinematic Hardening of a High Entropy Alloy

Olivier Bouaziz[1,2], Jongun Moon[3], Hyoung Seop Kim[3], Yuri Estrin[4,5]

[1]Laboratoire d'Etude des Microstructures et de Mécanique des Matériaux (LEM3), CNRS, Université de Lorraine, Arts et Métier Paris Tech, F 57000, Metz, France

[2]LABoratoire d'EXcellence DAMAS, Université de Lorraine, 57000, Metz, France

[3]Graduate Instite for Ferrous Technology, Pohang University of Science and Technology (POSTECH), Pohang 37673, Republic of Korea

[4]Department of Materials Science and Engineering, Monash University, Clayton, VIC 3800, Australia

[5]Department of Mechanical Engineering, The University of Western Australia, Crawley, WA 6009, Australia

Email: olivier.bouaziz@univ-lorraine.fr

Abstract

The contribution of kinematic hardening to the overall strain hardening of a high entropy alloy (HEA) was investigated for the first time ever. It was assessed for a single-phase equiatomic CoCrFeMnNi alloy based on a study of the Bauschinger effect. The observed occurrence of high back stresses signifies substantial kinematic hardening. We attribute it to the low probability of cross-slip in this HEA which, however, rises in the process of straining. A model that captures the mentioned effects was proposed and validated.

Keywords: high entropy alloys, isotropic hardening, kinematic hardening, back stress, Bauschinger effect

Alloying has long been used to confer desirable properties to materials. Typically, it involves the addition of relatively small amounts of secondary elements to a primary element. Over the past decade and a half, however, a new alloying strategy for designing new materials, referred to as high entropy alloys (HEAs), has emerged. It consists in combining multiple principal elements in high concentrations [1]. A surge in research activity in this area can be traced back to the publication of two seminal papers [2, 3] in 2004. To date, it has been reported that single- and multi-phase HEAs with a face-centered cubic (FCC) and/or body-centered cubic (BCC) crystal structure exhibit outstanding mechanical properties with their distinct deformation behavior [4] in the temperature range from cryogenic [5-8] to ambient [9-11] and elevated temperatures [12, 13]. Furthermore, excellent surface properties such as corrosion resistance [14-16], wear resistance [17, 18], and oxidation resistance [19] have boosted research in the field of HEAs.

Recently, several reports asserted that a superior combination of strength and ductility of heterostructured HEAs is due to high back stress or hetero-deformation-induced strengthening [20, 21]. Indeed, back stress in HEAs provides extra strengthening in addition to conventional mechanisms such as solid solution strengthening [22] and precipitation strengthening [23]. However, to the authors' knowledge there is no literature on back stress and the associated kinematic hardening in HEAs.

Kinematic hardening manifests itself in the Bauschinger effect: a reduction of the yield strength of an alloy upon a change in direction of loading. It is associated with a back stress, which is often disregarded in constitutive modelling of strength and plasticity of alloys. The significance of back stress for the constitutive behavior of alloys was highlighted in a recent publication [23]. This communication aims at elucidating the evolution of both principal

elements of strain hardening: isotropic hardening (associated with the evolution of the dislocation density) and the kinematic hardening (related to back stress) as exemplified by the Bauschinger effect studied for an equiatomic CoCrFeMnNi alloy.

An ingot of HEA $Co_{20}Cr_{20}Fe_{20}Mn_{20}Ni_{20}$ (at%) was prepared using vacuum induction melting in argon atmosphere. The purity of the alloying elements for casting was above 99.9%. The ingot was homogenized at 1100° C for 6 h in argon atmosphere, followed by water quenching. The surface of the homogenized ingot was mechanically milled in order to remove surface roughness and oxides. After that, cold rolling was performed with a thickness reduction from 7 mm to 1.5 mm. The cold-rolled plate was annealed at 800 or 1000° C for 1 h in argon atmosphere, followed by water quenching, to produce different grain sizes of the alloy, 4.6 µm and 18.2 µm, respectively.

Uniaxial tension and tension-compression tests on the annealed samples were carried out using an Instron 1361 equipment with a strain rate of 10^{-3} s^{-1}. An extensometer was attached to the gauge section of each specimen to measure engineering strain during the tests. The dog-bone shaped tensile specimens with a gauge length of 7.5 mm, a width of 6 mm, and a thickness of 1.5 mm were used. The tensile specimens were polished using up to 1200-grit SiC paper before the tests.

The deformation curves for samples of the alloy with two different grain sizes (corresponding to the different annealing regimes) are presented in Fig. 1. Using these experimental curves, it is possible to determine the back stress after pre-straining to different tensile strain from the equation [23]:

$$\sigma_b = \frac{\sigma - |\sigma_{y,f}|}{2}, \quad (1)$$

where σ is the flow stress after a tensile pre-strain and $\sigma_{y,f}$ is the yield stress in compression.

The evolution of the back stress along with the total flow stress for the HEA studied is drawn in Fig. 2, which shows that the back stress represents a sizeable part of the overall stress and that it contributes to strain hardening significantly. In general, high back stress was observed in multi-phase alloys and heterogeneous materials. While the microstructure of the HEA under investigation is a single phase, a high back stress was found. It can be conjectured that the elemental composition of the alloy inhibits cross-slip of dislocations and promotes planar slip.

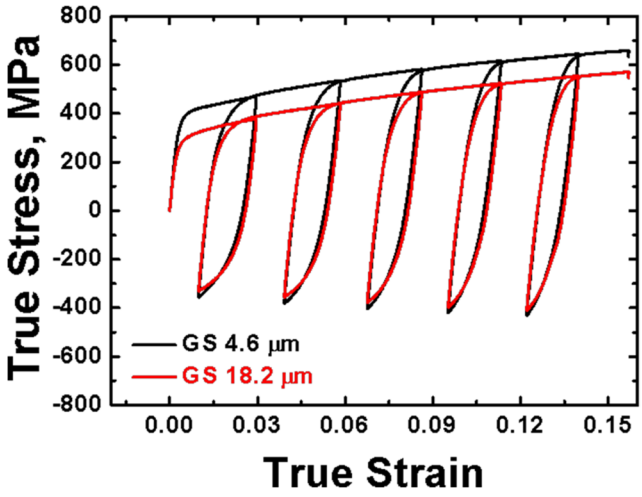

Fig. 1. Room temperature tension/compression tests for different pre-strains for two different values of the grain size.

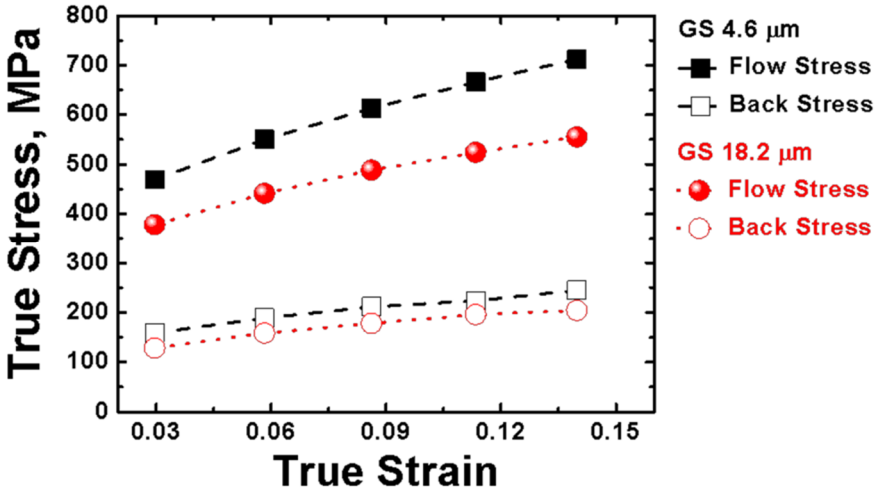

Fig. 2. Variation of the total flow stress and the back stress with strain for the two grain size values considered.

A model accounting for the effect of back stress on strain hardening in conventional alloys was proposed in Ref. [23]. It was shown to be well suited for a description of strain hardening of simple ferritic solid solutions. While being phenomenological in nature, the model is guided by physical considerations relating to dislocation kinetics. Here we demonstrate that the model works equally well for the HEA under consideration. Its main ingredients are as follows. The total flow stress is assumed to be the sum of two components: that associated with forest dislocations, σ_f, and the back stress, σ_b:

$$\sigma = \sigma_f + \sigma_b. \tag{2}$$

The changing balance between the isotropic hardening by the accumulation of forest dislocations and the kinematic hardening associated with the variation of back stress is given by the following evolution laws [24]:

$$\frac{d\sigma_f}{d\varepsilon} = \frac{M\alpha\mu b}{2\sqrt{\rho}} \cdot P \cdot \frac{d\rho}{d\varepsilon}, \tag{3}$$

$$\frac{d\sigma_b}{d\varepsilon} = \frac{M\alpha\mu b}{2\sqrt{\rho}} \cdot (1 - P) \cdot \frac{d\rho}{d\varepsilon}, \tag{4}$$

where M is the Taylor factor (M = 3.06 for FCC random texture), α is a constant in the Taylor equation relating the stress to the dislocation density ρ (set at 0.25), b is the magnitude of the dislocation Burgers vector ($b = 2.5 \cdot 10^{-10} m$), μ is the shear modulus ($\mu = 81\ GPa$), and P is the cross-slip probability ($0 \leq P \leq 1$).

It is seen from Eqs. (3) and (4) that both contributions to stress are given by a square root dependence on the dislocation density ρ (the Taylor relation). The partitioning of the stress into the isotropic hardening and the kinematic hardening contributions is governed by the cross-slip probability P. Strain hardening is thus controlled by the variation of ρ and P in the course of plastic deformation. In the original model [23] the evolution equation for the dislocation density is expressed as

$$\frac{d\rho}{d\varepsilon} = M\left(\frac{k}{b}\sqrt{\rho}\right) exp\left(-\beta P\sqrt{\rho}\right), \tag{5}$$

where k and β are model parameters to be identified from experiments. It should be noted that this heuristic equation recovers the classical Kocks-Mecking evolution equation if $\beta P\sqrt{\rho} \ll 1$, thus representing stage III strain hardening behavior, while also reflecting stage IV hardening for larger values of this quantity. For small grain size materials, when the grain size d influences the dislocation mean free path in a substantial way, a modification of this equation in the spirit of the model proposed in [24] is appropriate:

$$\frac{d\rho}{d\varepsilon} = M\left(\frac{1}{bd} + \frac{k}{b}\sqrt{\rho}\right) exp\left(-\beta P\sqrt{\rho}\right). \tag{6}$$

As the grain size of both batches of the alloy, corresponding to the two different heat treatment histories, was rather small, we used this extension of the original model.

Finally, the above set of the constitutive relations needs to be completed by an evolution equation for the cross-slip probability. The following form of this equation was used in [23] to account for the stress dependence of the evolution of P [25]:

$$\frac{dP}{1-P} = \frac{\sigma}{\sigma_c} d\epsilon, \tag{7}$$

where σ_c is a critical stress for cross-slip.

Relating the occurrence of kinematic hardening to the cross-slip probability of dislocations, *P*, in the way done in the original model [23], goes back to the work of Ibrahim and Embury [26] who established that solute solutions promote planar slip, which in turn gives rise to back stress. The mechanism for that can be associated with solute-induced reduction of the stacking fault energy which leads to a greater spacing between the Shockley partial dislocations into which a perfect dislocation splits, which makes recombination of the partials necessary for cross-slip more difficult [27]. Using the weight factors of *P* and *(1-P)* in the above partitioning the flow stress into the isotropic and kinematic parts captures this trend but is, of course, a simplistic *ad hoc* interpolation between the extreme cases of vanishing kinematic hardening and that entirely dominating the strain hardening behavior.

Figure 3 provides a comparison of the model calculations with the experimental data on the variation of the flow stress and the back stress determined in the way described above. The fitting was done by using an initial value of 0.1 for the cross-slip probability *P* (i.e., difficult cross-slip), setting σ_c at 400 MPa, and identifying the values of the parameters *k* and β as 0.016 m^{-1} and $2.5 \cdot 10^{-8}$ m, respectively. An excellent agreement between the measured and calculated stress-strain curves is not matched by the back-stress results, but the accord can still be considered as reasonably good, particularly as it improves with growing strain. The calculated R^2 values for the model validation were 0.99 for the flow stress and 0.15 for the back stress. It should be noted that the fitting was done for the best fit of the flow stress data.

The lower R^2 value for the back stress may be due to the use of different specimens to obtain tension and tension-compression curves in Fig. 1 and 3. A further substantiation of the good predictive capability of the model is provided by Fig. 4 where the data of Fig. 3 are re-cast in a plot showing the strain hardening rate, $\Theta = \partial\sigma/\partial\epsilon$, as a function of stress, which is a representation of the data more sensitive to the details of the model and the parameter values than the stress-strain curve. Both the common Kocks-Mecking plot, Fig. 4a, and the $\Theta \cdot (\sigma - \sigma_y)$ vs. $(\sigma - \sigma_y)$ diagram, specifically suited for the extended version of the model [28], Fig. 4b, are displayed. Again, a good accord between the model calculations and the experimental data within the strain range of uniform tensile elongation has been established.

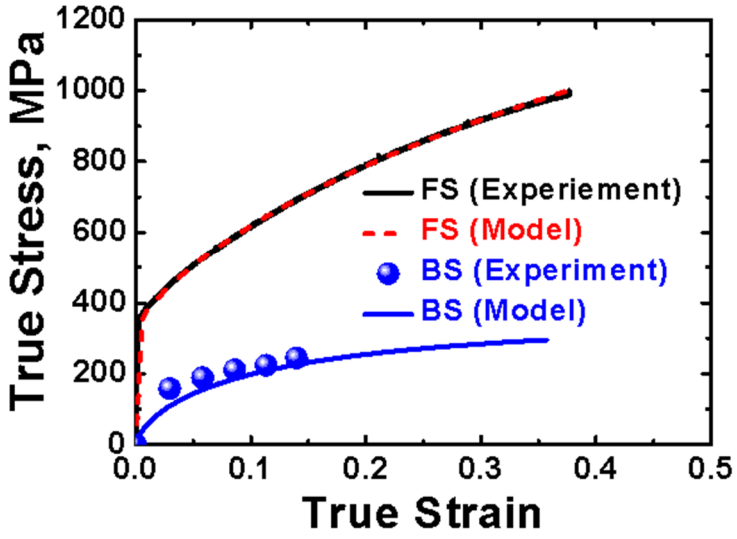

Fig. 3. Comparison between experiment and modelling for the flow stress (colour lines) and back stress (symbols for the experiment and grey solid line for modelling) for 4.6 µm grain size. FS and BS represent flow stress and back stress, respectively.

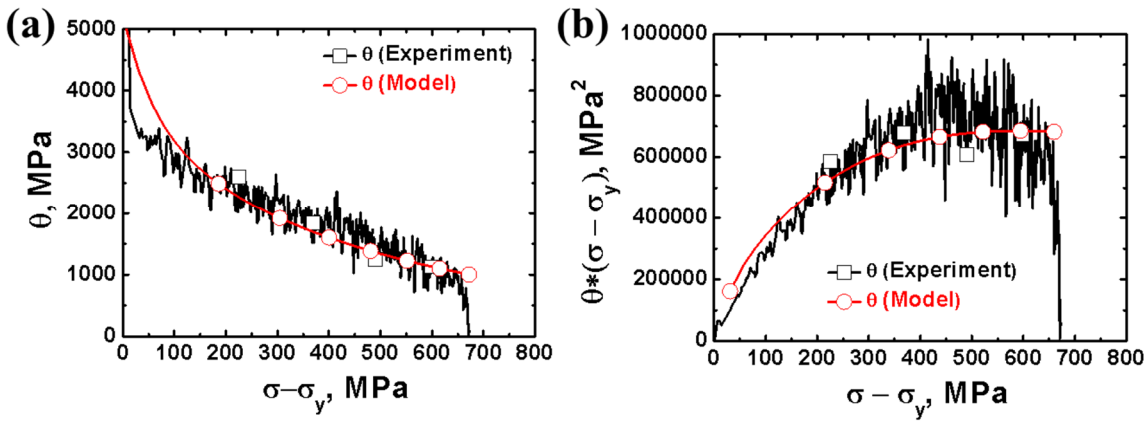

Fig. 4. Comparison between experiment and modelling in (a) a Kocks-Mecking plot and (b) in a $\Theta \cdot (\sigma - \sigma_y)$ vs. $(\sigma - \sigma_y)$ plot for the grain size of 4.6 µm.

Having confidence in the predictive capability of the model verified in this exercise, we can now look at the variation of the cross-slip probability given by Eq. (7) during straining and assess it quantitatively. The strain dependence of P is shown in Fig. 5. A strong increase in the cross-slip probability in the process of plastic deformation, which is at the core of the tendency of the back stress towards saturation seen from Eq. (4), is evident from this diagram. A more rapid saturation of σ_b compared to that of the overall flow stress σ indicates that the relative role of the kinematic hardening diminishes with the progress of straining.

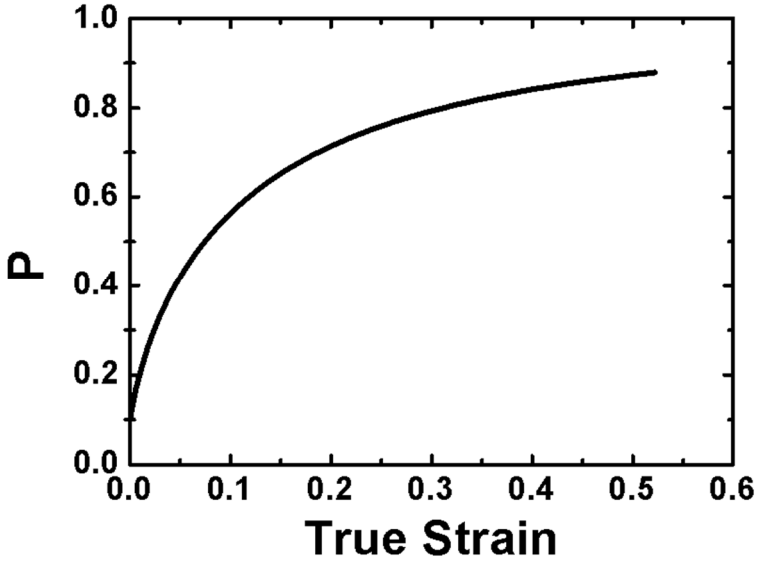

Fig. 5. Evolution of the cross-slip probability *P* in the process of straining.

The applicability of the present model to the equiatomic HEA CoCrFeMnNi that has been established in this work does not warrant, of course, its general validity for HEAs. That is why it appears necessary to study the effect of the HEA composition on the stacking-fault energy and, through its effect on cross-slip probability and the planarity of dislocation slip, on the strain hardening behavior.

For the first time ever, the back stress (associated with kinematic hardening) has been measured for a high-entropy alloy using the Bauschinger effect in tension-compression tests. The data obtained experimentally for an equiatomic HEA CoCrFeMnNi were compared with calculations based on a phenomenological proposed earlier, which is fairly general and turned out to be valid for the HEA considered. We believe that it will also be applicable to a broader range of HEAs. Its further extension should include compositional effects, which can be introduced through the cross-slip probability function P. We envisage this as the next step of research in this area.

Acknowledgment

This research was supported by Creative Materials Discovery Program through the National Research Foundation of Korea (NRF) funded by Ministry of Science and ICT (2016M3D1A1023384).

References

[1] E. P. George, D. Raabe, R. O. Ritchie, High-entropy alloys, *Nature Review Mater.* **4** (2019) 515.

[2] J. W. Yeh, S.-K. Chen, S.-J. Lin, J.-Y. Gan, T.-S. Chin, T.-T. Shun, C.-H. Tsau, S.-Y. Chang, Nanostructured high-entropy alloys with multiple principal elements: novel alloy design concepts and outcomes, *Adv. Eng. Mater.* **6** (2004) 299-303.

[3] B. Cantor, I. T. H. Chang, P. Knight, A. J. B. Vincent, Microstructural development in equiatomic multicomponent alloys, *Mater. Sci. Eng. A* **375** (2004) 213-218.

[4] J. Brechtl, S. Chen, C. Lee, Y. Shi, R. Feng, X. Xie, D. Hamblin, A. M. Coleman, B. Straka, H. Shortt, R. J. Spurling, P. K. Liaw, A Review of the Serrated-Flow Phenomenon and Its Role in the Deformation Behavior of High-Entropy Alloys, *Metals* **10** (2020) 1101.

[5] H. Kwon, J. Moon, J. W. Bae, J. M. Park, S. Son, H.-S. Do, B.-J. Lee, H. S. Kim, Precipitation-driven metastability engineering of carbon-doped CoCrFeNiMo medium-entropy alloys at cryogenic temperature, *Scripta Mater.* **188** (2020) 140-145.

[6] J. Moon, J. M. Park, J. W. Bae, N. Kang, J. Oh, H. Shin, H. S. Kim, Hetero-deformation-induced strengthening by twin-mediated martensitic transformation in an immiscible medium-entropy alloy, *Scripta Mater.* **186** (2020) 24-28.

[7] P. Sathiyamoorthi, J. Moon, J. W. Bae, P. Asghari-Rad, H. S. Kim, Superior cryogenic tensile properties of ultrafine-grained CoCrNi medium-entropy alloy produced by high-pressure torsion and annealing, *Scripta Mater.* **163** (2019) 152-156.

[8] J. W. Bae, J. B. Seol, J. Moon, S. S. Sohn, M. J. Jang, H. Y. Um, B.-J. Lee, H. S. Kim, Exceptional phase-transformation strengthening of ferrous medium-entropy alloys at cryogenic temperatures, *Acta Mater.* **161** (2018) 388-399.

[9] L. Lin, X. Xian, Z. Zhong, Y. Wu, P. K. Liaw, Microstructure stability and its influence on the mechanical properties of $CrMnFeCoNiAl_{0.25}$ high entropy alloy, *Met. Mater. Int.* **26** (2020) 1192.

[10] S.-H. Joo, J. W. Bae, W.-Y. Park, Y. Shimada, T. Wada, H. S. Kim, A. Takeuchi, T. J. Konno, H. Kato, I. V. Okulov, Beating thermal coarsening in nanoporous materials via high-entropy design, *Adv. Mater.* **32** (2020) 1906160.

[11] F. Prusa, M. Cabibbo, A. Šenková, V. Kučera, Z. Veselka, A. Školáková, D. Vojtěch, J. Cibulková, J. Čapek, High-strength ultrafine-grained CoCrFeNiNb high-entropy alloy prepared by mechanical alloying: Properties and strengthening mechanism, *J. Alloys Compd.* **835** (2020) 155308.

[12] N. T.-C. Nguyen, P. Asghari-Rad, P. Sathiyamoorthi, A. Zargaran, C. S. Lee, H. S. Kim, Ultrahigh high-strain-rate superplasticity in a nanostructured high-entropy alloy, *Nature Commun.* **11** (2020) 2736.

[13] L. Lin, X. Xian, Z. Zhong, Y. Wu, P. K. Liaw, Microstructure stability and its influence on the mechanical properties of $CrMnFeCoNiAl_{0.25}$ high entropy alloy, *Met. Mater. Int.* **26** (2020) 1192.

[14] Y. Zhang, T. T. Zuo, Z. Tang, M. C. Gao, K. A. Dahmen, P. K. Liaw, Z. P. Lu, Microstructures and properties of high-entropy alloys, *Prog. Mater. Sci.* **61** (2014) 1-93.

[15] C. P. Lee, C. C. Chang, Y. Y. Chen, J. W. Yeh, H. C. Shih, Effect of the aluminium content of $Al_xCrFe_{1.5}MnNi_{0.5}$ high-entropy alloys on the corrosion behaviour in aqueous environments, *Corros. Sci.* **50** (2008) 2053-2060.

[16] Y. L. Chou, J. W. Yeh, H. C. Shih, The effect of molybdenum on the corrosion behaviour of the high-entropy alloys Co1.5CrFeNi1.5Ti0.5Mox in aqueous environments, *Corros. Sci.* **52** (2010) 2571-2581.

[17] C. Huang, Y. Zhang, R. Vilar, J. Shen, Dry sliding wear behavior of laser clad TiVCrAlSi high entropy alloy coatings on Ti–6Al–4V substrate, *Mater. Des.* **41** (2012) 338-343.

[18] M.-H. Chuang, M.-H. Tsai, W.-R. Wang, S.-J. Lin, J.-W. Yeh, Microstructure and wear behavior of $Al_xCo_{1.5}CrFeNi_{1.5}Ti_y$ high-entropy alloys, *Acta Mater.* **59** (2011) 6308-6317.

[19] O. A. Waseem, H. J. Ryu, Combinatorial synthesis and analysis of $Al_xTa_yV_z$-$Cr_{20}Mo_{20}Nb_{20}Ti_{20}Zr_{10}$ and $Al_{10}CrMo_xNbTiZr_{10}$ refractory high-entropy alloys: Oxidation behaviour, *J. Alloys Compd.* **828** (2020) 154427.

[20] E. Ma, X. Wu, Tailoring heterogeneities in high-entropy alloys to promote strength–ductility synergy, *Nat. Commun.* **10** (2019) 5623.

[21] P. Shi, W. Ren, T. Zheng, Z. Ren, X. Hou, J. Peng, P. Hu, Y. Zhong, P. K. Liaw, Enhanced strength–ductility synergy in ultrafine-grained eutectic high-entropy alloys by inheriting microstructural lamellae, *Nat. Commun.* **10** (2019) 489.

[22] I. Toda-Caraballo, A general formulation for solid solution hardening effect in multicomponent alloys, *Scripta Mater.* **127** (2017) 113-117.

[23] I. Basu, J. Th. M. De Hosson, Strengthening mechanisms in high entropy alloys: Fundamental issues, *Scripta Mater.* **187** (2020) 148-156.

[24] O. Bouaziz, D. Barbier , J.D. Embury, G. Badinier, An extension of the Kocks–Mecking model of work hardening to include kinematic hardening and its application to solutes in ferrite, *Phil. Mag.* **93** (2013) 247-255.

[25] Y. Estrin, H. Mecking, A unified phenomenological description of work hardening and creep based on one-parameter models, *Acta Metall.* **32** (1984) 57-70.

[26] N. Ibrahim, J. D. Embury, The Bauschinger effect in single phase b.c.c. materials, *Mater. Sci. Eng.* **19** (1975) 147-149.

[27] Y. Estrin, Dislocation-density–related constitutive modeling, in: A. Krauss, K. Krauss (Eds.), Unified constitutive laws of plastic deformation, Academic Press, 1966, pp. 69-106.

[28] W. Püschl, Models for dislocation cross-slip in close-packed crystal structures: a critical review, *Prog. Mater. Sci.* **47** (2002) 415-461.

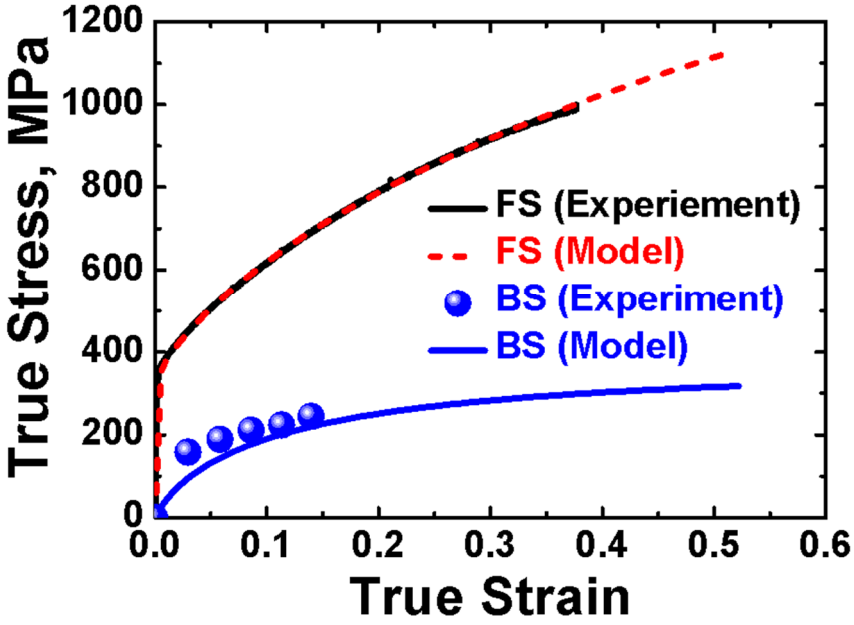

Fig. Comparison between experiment and modelling for the flow stress (colour lines) and